AIAA JOURNAL
Vol. 32, No. 2, February 1994

Experimental, Analytical, and Computational Methods Applied to Hypersonic Compression Ramp Flows

G. Simeonides*
von Kármán Institute for Fluid Dynamics, B-1640 Rhode St-Genèse, Belgium
W. Haase†
Dornier Luftfahrt GmbH, D-88039 Friedrichshafen 1, Germany
and
M. Manna‡
von Kármán Institute for Fluid Dynamics, B-1640 Rhode St-Genèse, Belgium

Experimental data on fully laminar and transitional shock-wave/boundary-layer interactions in two-dimensional compression corners are provided and used for the validation of two full Navier-Stokes solvers, as well as for checking the capabilities and limitations of simple analytical prediction methods. Viscous pressure interaction, free interaction, and inviscid oblique shock theory are found to predict well the pressure levels on the flat plate upstream of the interaction, within the separated region, and downstream of the interaction, respectively. The reference temperature theory is found to perform well in attached flow regimes both upstream and downstream of the interaction region and to provide the basis for a universal peak heating correlation law. Full Navier-Stokes computations are necessary, however, to predict the extent of the interaction region and the associated influence on the pressure distribution (control effectiveness) as well as the detailed heat transfer distribution. To achieve this, very fine gridding coupled with the use of strict convergence criteria (based on the evolution of the location of the separation point rather than on standard density residuals) is shown to be necessary. It is finally shown that, although sophisticated turbulence models need to be further developed before the detailed characteristics of fully turbulent shock-wave/boundary-layer interactions may be predicted, transitional interactions (where transition typically occurs in the neighborhood of reattachment) may be adequately handled by algebraic turbulence models "switched on" just downstream of reattachment.

Nomenclature

C	= Chapman-Rubesin linear viscosity law constant
c_f	= skin friction coefficient [Eq. (2)]
c_H	= heat transfer coefficient [Eq. (3)]
c_p	= specific heat at constant pressure
K_p	= pressure coefficient [Eq. (1)]
L	= distance of hinge line from leading edge
L_{pk}	= growth length of reattaching boundary layer to location of peak heating
M	= Mach number
$N_{L_{sep}}$	= number of mesh points along the wall in the separated region
$N_{\delta sep}$	= number of mesh points in the boundary layer at separation
p	= pressure
$\dot{q}_s$	= heat transfer rate into model surface
Re	= Reynolds number
Re_{unit}	= unit Reynolds number (per meter)
T	= temperature
u	= velocity
x	= distance from leading edge
α	= ramp deflection angle
α_s	= deflection angle of dividing streamline
γ	= ratio of specific heats
δ_s	= shear layer thickness at reattachment
ρ	= density
τ_w	= wall shear stress

Subscripts

e	= at edge of boundary layer
pk	= at peak heating
r	= recovery (adiabatic wall)
reat	= at reattachment
ref	= reference boundary layer
sep	= at separation
w	= wall
0	= reservoir (total)
∞	= freestream

Superscript

*	= at Eckert's reference temperature

I. Introduction

RECENT years have seen the development of a number of concepts for novel space transportation systems with widely varying mission requirements that, however, all aim to optimize the performance of such systems and to provide easy and cost-effective access to space. Many of the proposed systems rely on the concept of reusability, which, effectively, translates to lifting re-entry space planes similar to the operational U.S. Space Shuttle Orbiter. Others aim for a lifting ascent as well, with the aid of airbreathing or rocket propulsion, and for an overall operational performance and simplicity similar to that of current commercial airliners.

One of the most critical areas in the design of hypersonic aircraft is the design of control surfaces,[1,2] where it is well known that strong shock-wave/boundary-layer interactions occur upon their deflection, giving rise to a loss of control effectiveness and high heating rates.[3-5] As a consequence, a significant worldwide research effort has been undertaken to provide a better understanding of the relevant flow processes and reliable prediction techniques, with particular emphasis placed on the development and validation of computational fluid dynamics (CFD) methods.[2,5-8]

Received July 10, 1992; revision received Oct. 21, 1992; accepted for publication Nov. 9, 1992.

*Research Fellow, Aeronautics/Aerospace Department. Ch. de Waterloo 72. Member AIAA.
†Senior Research Scientist, Department LREV 32.
‡Research Assistant, Turbomachinery Department, Ch. de Waterloo 72.

Two categories of hypersonic space planes may be distinguished in the modern trends. First, there are lifting re-entry vehicles, such as the European Hermes space plane and the U.S. HL-20 Personnel Launch System, which are very similar to the Space Shuttle Orbiter, although their small scale poses severe heating problems in nose and leading-edge areas and gives rise to significant uncertainties in the design of control surfaces as the laminar (due to the small scale) oncoming boundary layers are by far more prone to separation in regions of shock-wave/boundary-layer interaction than turbulent boundary layers. Furthermore, transition is often promoted by the process of shock-wave laminar boundary-layer interaction, a phenomenon that has so far received limited attention (because of its inherent difficulties) despite its relevance to efficient control surface design.

The second category of hypersonic space planes includes lifting ascent/re-entry vehicles, such as the U.S. National Aerospace Plane and the German Sänger. The associated high Reynolds numbers encountered during the lifting ascent of such vehicles are expected to yield turbulent flows over many of their wetted surfaces, so that the accurate modeling of turbulence[9] becomes very important in the efficiency of the design.

The present paper addresses the deflected control surface problem, as simulated by flat-plate/two-dimensional compression ramp configurations (Fig. 1), at Mach numbers of 6 and 14 with Reynolds numbers to the hinge line in the range 0.3×10^6 to 2.5×10^6 and wall-to-total temperature ratios between 0.1 and 0.85. The test cases considered involve ramp deflection angles between 7.5 and 25 deg approached by laminar boundary layers which, in the laboratory, give rise to two-dimensional fully laminar or transitional shock-wave/boundary-layer interactions, including cases with extensive separation. Fully turbulent interactions, with the inherent need for turbulence modeling within separated flow regions, are not considered.

In what follows, examples of experimental, analytical, and computational results are discussed, emphasizing validation issues. A synthesis that may provide useful hints to the designer of control surfaces is also presented.

II. Description of the Experiments

Experimentally, the problem has been treated in the two hypersonic wind tunnels of the von Kármán Institute (VKI), namely, the Mach 6 H-3 blowdown and the Mach 14 Longshot heavy piston gun tunnels.[10] Surface pressure and heat transfer distributions have been measured by a variety of measurement techniques,[10] and the data have been complemented by schlieren and surface oil flow and sublimation visualizations. Repeatability and flow establishment (in the Longshot intermittent tunnel) have been demonstrated. Two-dimensionality has been checked for the cases chosen for code validation purposes. Specifically, the insensitivity of centerline pressure and heat transfer distributions to the use of side plates covering the recirculation zone has been demonstrated,[11,12] which is a necessary and sufficient condition for two-dimensionality in the centerline region of the model insofar as finite span effects are concerned. The uncertainties in the measurements and in the definition of the test conditions have been determined to reflect the current state of the art in hypersonic testing.[10-15]

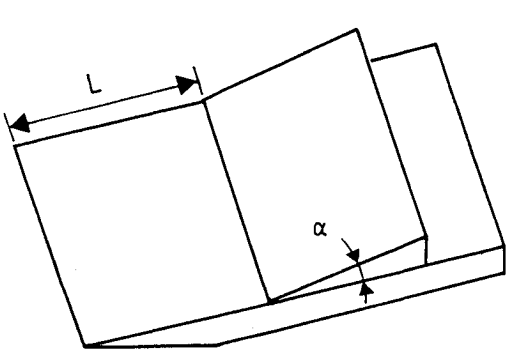

Fig. 1 Flat plate/two-dimensional ramp geometry.

Three test cases are considered for the purposes of code validation, all involving flat-plate/two-dimensional ramp configurations with the flat plate at zero incidence and a nominally sharp leading edge tested in perfect gas flow conditions. First, a Mach 6 (±1% nonuniformity, particularly evident near the axis of the tunnel) fully laminar test case with a ramp deflected to 7.5 deg and the hinge line located at 40 mm downstream of the leading edge is considered.[16] The unit Reynolds number is 10×10^6/m (±10% uncertainty/nonrepeatability), the total temperature of the flow is 470 K (±3% uncertainty/nonrepeatability), and the model surface temperature is equal to the adiabatic wall temperature. The uncertainty of the surface pressure measurements is estimated to ±5% that, combined with the aforementioned flowfield nonuniformity, may yield an overall uncertainty in the pressure coefficient of the order of ±10%. The mean model leading-edge thickness in the experiment was 80 μm, which at Mach 6 has a negligible effect on the data.[16]

The second and third test cases involve flat-plate/15-deg ramp configurations at Mach 14 (±1.5% uncertainty/nonrepeatability), with a unit Reynolds number of 6.5×10^6/m (±13% uncertainty/nonrepeatability), an equivalent perfect gas total temperature of 2385 K (±9% uncertainty/nonrepeatability), and a model surface temperature of 295 K.[11,13-15] The Mach number nonuniformity in the test section is within the uncertainty/nonrepeatability band. In the second test case the hinge line is located at 70 mm downstream of the model's leading edge, giving rise to a fully laminar shock-wave/boundary-layer interaction. In the third test case the hinge line is located at 200 mm downstream of the model's leading edge, and laminar-turbulent transition is exhibited in the close vicinity of reattachment. The measurements are characterized by uncertainty levels of ±16% on the pressure coefficient on the low-pressure flat-plate part of the model, ±6% on the pressure coefficient on the ramp, and ±13% on the heat transfer coefficient over the entire measurement domain. These estimates reflect the uncertainties in the measurements and in the determination of the relevant flow conditions, as well as the contribution of flowfield nonuniformity.

The model leading-edge thickness in the experiment corresponding to the second test case was characterized by a mean value of 70 μm and a spanwise variation of ±10 μm. For the third test case, the pressure data were collected over a model with a leading-edge thickness distribution of 55 μm ± 3 μm and the heat transfer data over a model with a leading-edge thickness distribution of 35 μm ± 10 μm.[11] Contrasting the pressure data with the heat transfer data in the third test case, it has been concluded that such model leading-edge thickness variations have little effect on the location and extent of the interaction.

Three criteria have been employed to detect the occurrence of laminar-turbulent transition in the Mach 14 experiments: the presence of a granular structure within the boundary or shear layer in schlieren photographs, the noise pattern in 24-kHz surface temperature time traces, and the comparison of the measured heat transfer data downstream of the interaction region to the reference temperature predictions discussed in Sec. III. For the first test case at Mach 6, the low strength interaction over the 7.5-deg ramp configuration has been determined to be fully laminar[16] on the basis of criteria established by Ginoux.[17]

For the comparisons that follow, the data are presented in coefficient form. The pressure coefficient is defined as

$$K_p = \frac{p - p_\infty}{\frac{1}{2}\gamma p_\infty M_\infty^2} \tag{1}$$

The skin friction coefficient is defined as

$$c_f = \frac{\tau_w}{\frac{1}{2}\rho_\infty u_\infty^2} \tag{2}$$

The heat transfer coefficient is defined as a modified Stanton number of the form

$$c_H = \frac{\dot{q}_s}{\rho_\infty u_\infty c_{p\infty}(T_0 - T_w)} \tag{3}$$

Finally, it is noted that a much larger number of experiments[11,12,15] have been conducted at Mach numbers of 6 and 14, and the results have been successfully compared with the analytical predictions discussed in Sec. III. Although the bulk of this database involves transitional shock-wave/boundary-layer interactions, which have not been used for code validation purposes for the moment, the data have served the development and validation of a peak heating correlation that is discussed later. In addition, they have provided evidence on the level of striation heating that is often observed in reattaching flows and have allowed for the determination of an upper limit on the heat transfer rate that is briefly addressed in Sec. V.[11,12]

III. Description of the Analytical Predictions

Analytically, it has been found that viscous pressure interaction theory,[18] combined with the blast wave theory prediction for the pressure induced by a small leading-edge bluntness,[19] performs satisfactorily in predicting the pressure distribution over the flat-plate part of the models upstream of the onset of the interaction. Free interaction theory[4] has also been found to predict well the plateau pressure level within the separated flow region.

The reference temperature method[20,21] has been successfully employed to predict the heat transfer distributions over attached flow regions, that is, upstream and downstream of the interaction region, including the high heating rates on the deflected ramp downstream of reattachment for both laminar and turbulent reattachment cases. The general reference temperature result is given by

$$c_H(Re_{\infty,x})^n = \frac{A}{s}\left(\frac{u_e p_e}{u_\infty p_\infty}\right)^{1-n}\left(\frac{T_\infty}{T^*}\right)^{1-2n} \times (C^*)^n\left(\frac{T_r - T_w}{T_0 - T_w}\right) \tag{4}$$

where $n = 0.5$, $A = 0.332$, and $s = Pr^{2/3}$ for a laminar boundary layer, and $n = 0.2$, $A = 0.0296$, and $s = 1$ for a turbulent boundary layer at high Mach numbers.

Now, application of Eq. (4) to a reference boundary layer, typically taken as one over a flat plate at zero incidence with freestream edge conditions and with the origin of the boundary layer at the leading edge of the flat plate, gives a reference value for the heat transfer rate (or coefficient) that would occur, in the absence of an interaction, at the location of peak heating on the respective deflected ramp. An estimate for the heat transfer coefficient at the location of peak heating, corresponding to the peak ramp pressure and with the origin of the ramp boundary layer also taken at the leading edge of the flat plate, may be similarly obtained from Eq. (4). Finally, if the thinning of the reattaching ramp boundary layer, caused by the reattachment compression, is accounted for by taking its virtual origin in the vicinity of the reattachment point rather than at the leading edge of the flat plate, then the growth length at the location of peak heating used in the Reynolds number term of Eq. (4) is L_{pk} rather than x_{pk}.

Taking the ratio of the latter peak heating estimate to the former reference value yields a theoretically based correlation for peak heating[11,22]:

$$\frac{\dot{q}_{pk}}{\dot{q}_{\text{ref}}} = B(Re^*_{x_{pk}})^a\left(\frac{p_{pk}u_{pk}}{p_{\text{ref}}u_{\text{ref}}}\right)^{1-n}\left(\frac{x_{pk}}{L_{pk}}\right)^n \tag{5}$$

with $a = 0$, $B = 1$, and $n = 0.5$ for fully laminar interactions with a laminar reference level, $a = 0$, $B = 1$, and $n = 0.2$ for fully turbulent interactions with a turbulent reference level, and $a = 0.3$, $B = 0.072$, and $n = 0.2$ for turbulent peak heating with a laminar reference level.

The length scale L_{pk}, that is, the effective growth length of the reattaching boundary layer, has been found[11,12] to be well approximated by the method proposed by Bushnell and Weinstein[23] as

$$L_{pk} = \frac{\delta_s}{\sin(\alpha - \alpha_s)} \tag{6}$$

where the thickness of the shear layer at the reattachment point δ_s may be computed by the compressible Blasius result, and the deflection angle of the separated shear layer from free interaction theory. The velocity ratio u_{pk}/u_{ref} may often be neglected, inducing an error typically of the order of 10%, and the pressure ratio p_{pk}/p_{ref} may be approximated by the inviscid pressure ratio through a single inviscid shock or a two-shock system (separation shock plus reattachment shock) or as the pressure ratio through an isentropic compression. The use of a reference Reynolds number to correlate turbulent ramp data to a laminar flat-plate reference heating level is also noted.

For fully laminar or fully turbulent interactions and neglecting the velocity ratio term, Eq. (5) reduces to

$$\frac{\dot{q}_{pk}}{\dot{q}_{\text{ref}}} = \left(\frac{p_{pk}}{p_{\text{ref}}}\right)^{1-n}\left(\frac{x_{pk}}{L_{pk}}\right)^n \tag{7}$$

which is equivalent to the numerous pressure interaction semi-empirical peak heating correlations summarized by Hung[24] but includes an additional term that represents the relative growth lengths of the reference and ramp boundary layers. It is recalled that such semi-empirical correlations have been very successful for fully turbulent interactions with a value of the exponent $(1 - n)$ close to 0.8 (that is the theoretical reference temperature value) but have been a complete failure for fully laminar interactions where exponents $(1 - n)$ in the range 0.7–1.9 have been determined[24] as opposed to the theoretical value of 0.5. In addition, correlations for peak heating in transitional interactions (with a turbulent ramp peak heating level and a laminar reference level), such as the one proposed by Hung and Barnett,[25] have also presented severe limitations in their performance.[12] Accounting for the thinning of the reattaching boundary layer caused by the interaction process in the form of Eqs. (5) or (7), on the other hand, has been found to provide the grounds for a universal peak heating correlation in regions of both two- and three-dimensional shock-wave/boundary-layer interactions.[11,12,22] The results of this improved correlation are presented in Sec. V.

Finally, what is currently not possible with simple semi-empirical and/or analytical methods is the accurate prediction of the extent of the separated region and the location of the separation point, since a universal correlation law has yet to be developed. This, in turn, makes the incorporation of CFD methods in the design process necessary, particularly insofar as the prediction of control effectiveness, which strongly depends on the geometric characteristics of the interaction (as opposed to peak heating), is concerned. Clearly, full Navier-Stokes solvers need to be critically validated before being relied upon by the designer, and this forms one of the primary objectives of the present paper.

IV. Description of the Computations

Computationally, the problem of shock-wave/boundary-layer interaction in compression corners has been treated by two Navier-Stokes solvers, one developed at Dornier[26–30] and one at the VKI.[31–33] In both codes, the two-dimensional unsteady full Navier-Stokes equations are integrated by means of time-marching finite volume shock-capturing methods based on cell-centered unknowns. The discretization of the convective terms is based on either a central (for the Dornier code) or

an upwind (for the VKI code) evaluation of the cell face fluxes. A standard nonlinear blend of second- and fourth-order artificial dissipation terms is employed to stabilize the central discretizations in the Dornier code. The VKI solver makes use of the flux difference splitting technique to evaluate the cell face fluxes; higher order schemes coupled with total variation diminishing (TVD) properties are implemented on the basis of the MUSCL approach. Both codes employ multistage Runge-Kutta integration schemes for the time discretization. The Cebeci-Smith turbulence model[34] is implemented in the Dornier code together with a transition "switch." The boundary-layer length scales are computed by the method proposed by Stock and Haase.[35]

The time evolution of the numerical solutions is, in both codes, monitored by means of an L_2 norm of the normalized density residuals. An overall decay of the residuals by three to four orders of magnitude is generally considered to yield a satisfactory steady-state solution. However, the extent of the separated region and the location of the separation point have exhibited a considerable sensitivity to further reduction in the residuals. Therefore, the establishment of the steady-state location of the separated point is believed to be a more appropriate convergence criterion, as will be discussed later. Still, it is noted that such an approach is likely to yield significant increases in computational time when noting the asymptotic behavior of convergence histories.

The Mach 6, 7.5-deg ramp test case has been computed by both codes. The Dornier computations have been conducted on a series of four meshes to check that the solution is independent of further grid refinement. The four mesh levels, employed with two multigrid (V) cycles, involve a total number of points of 62×12, 124×24, 248×48, and 496×96; in the finer mesh, the normal mesh size at the wall was 5×10^{-6} m. The VKI computation has been performed on 190×60 mesh points, with the normal mesh size at the wall set to 6.7×10^{-5} m. It is noted that the computational domain in the Dornier computations extended to 120 mm downstream of the leading edge as opposed to 80 mm in the VKI computations.

The fully laminar Mach 14, 15-deg ramp test case has also been computed with both codes. The Dornier computations again include an extensive grid dependence study with computations performed on meshes with 44×20, 88×40, 176×80, and 352×160 points. The wall normal stepsize in the finer mesh was again 5×10^{-6} m. The VKI computations have been performed at two mesh levels, namely with 84×30 and 190×60 mesh points. The first normal stepsize at the wall in the case of the finer grid was 3×10^{-5} m. The computational domain in the Dornier computations and in the coarse grid VKI computations extended to 250 mm downstream of the model leading edge. The fine grid VKI computations were performed over a length of 210 mm from the model leading edge.

Lastly, the transitional Mach 14 test case, with the hinge line of the 15-deg ramp located at 200 mm downstream of the model leading edge, has been computed only by the Dornier code. Fully laminar computations have been performed in a mesh series with 61×31, 124×62, and 248×124 mesh points. An additional mesh of 248×64 points has been employed to perform fully laminar and fully turbulent computations, as well as to check the influence of "switching on" the turbulence model just downstream of the laminar reattachment (note that transition in this experiment was detected to occur in the close vicinity of reattachment). In the latter case, the first wall normal stepsize was 5×10^{-5} m. The computational domain for this test case extended to 400 mm downstream of the model leading edge.

Table 1 Mesh resolution

Test case	Code	Mesh level	N_{Lsep}	$N_{\delta sep}$
Case 1	VKI	190 × 60	51	20
Mach 6	DORNIER	125 × 25	13	13
7.5 deg ramp	DORNIER	249 × 49	50	26
	DORNIER	497 × 97	103	53
Case 2	VKI	84 × 30	15	13
Mach 14	VKI	190 × 60	43	28
forward	DORNIER	89 × 41	16	28
15 deg ramp	DORNIER	177 × 81	43	55
	DORNIER	353 × 161	92	109
Case 3	DORNIER	62 × 31	no	sep.[a]
Mach 14	VKI	124 × 62	51	43
rear	DORNIER	248 × 124	84	87
15 deg ramp	DORNIER	248 × 64	80	35

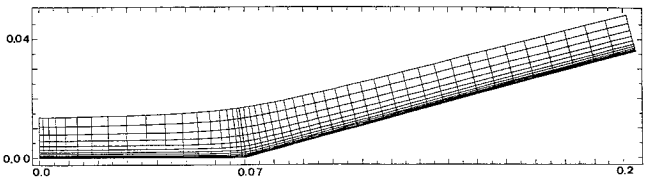

Fig. 2 Coarsened version of VKI 190 × 60 grid employed in the Mach 14 forward ramp computation.

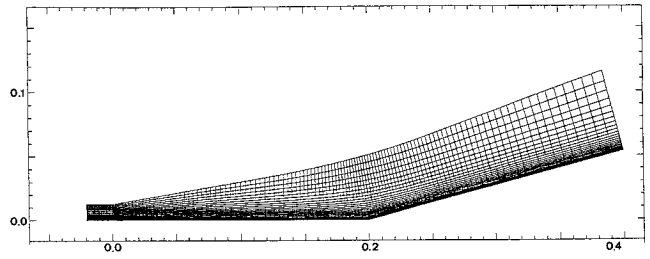

Fig. 3 Coarsened version of Dornier 248 × 64 grid employed in the Mach 14 rear ramp computation.

More information about the mesh resolution achieved in the various computations discussed herein is provided in Table 1. The number of mesh points included in the boundary layer at the separation point and the number of mesh points between the predicted separation and reattachment points are given as representative of the mesh resolution in the wall normal and streamwise directions, respectively.

The grids employed in the present study are illustrated in Figs. 2 and 3. Figure 2 shows a coarsened version of the fine 190×60 VKI grid employed in the second test case with the Mach 14 forward 15-deg ramp. Figure 3 shows a coarsened version of the 248×64 Dornier mesh employed in the third test case with the Mach 14 rear 15-deg ramp. The Dornier meshes were generated by an algebraic grid generation technique in which the outer boundary of the meshes was fitted close to the shock shape to optimize the mesh point distribution in the computational domain. The mesh lines were geometrically stretched in the wall normal direction. The VKI grids were generated by an analytic technique based on potential theory. In this case, orthogonal and smooth meshes are warranted, but a roughly constant normal extent of the mesh is imposed over the entire length of the computational domain (apart from the vicinity of the hinge line). The mesh lines were exponentially stretched in the wall normal direction.

V. Discussion of Results

A. Experiments vs Analytical Predictions

Typical pressure distributions measured along the centerline of the flat plate and flat-plate/15- and 25-deg ramp configurations at Mach 14 are shown in Fig. 4. The flat-plate data are compared with the combined viscous pressure interaction[18] and blast wave bluntness[19] predictions. Also shown are the free interaction predictions for the plateau pressure level[4] and the inviscid ramp pressure level obtained from oblique shock theory. The "peak" ramp pressure levels, too, have been estimated from oblique shock theory on the assumption of a two-shock system, where the strength of the separation shock

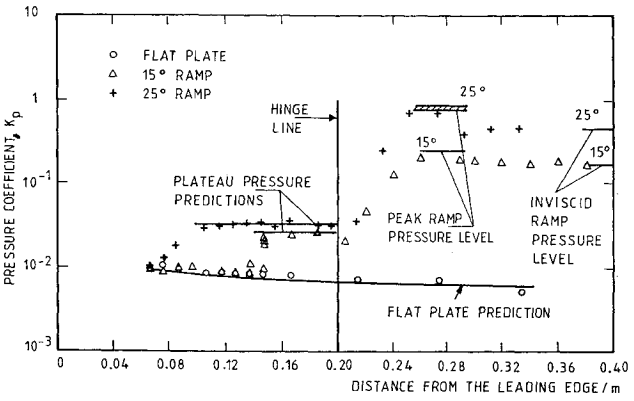

Fig. 4 Measured pressure distributions over flat plate and flat plate/2D ramp configurations at Mach 14 and $Re_{unit} = 6.5 \times 10^6$/m, and comparison with anayltical predictions.

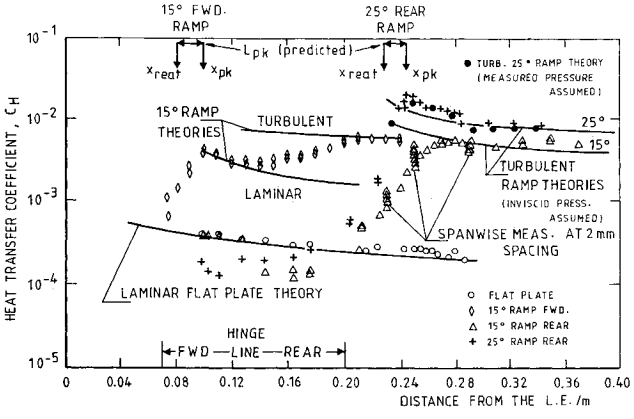

Fig. 5 Measured heat transfer distributions over flat plate and flat plate/2D ramp configurations at Mach 14 and $Re_{unit} = 6.5 \times 10^6$/m, and comparison with anayltical predictions.

gives the predicted plateau pressure level. Clearly, all predictions are in good agreement with the measurements.

Typical measured heat transfer distributions along the centerline of the flat plate and flat-plate/15- and 25-deg ramp configurations at Mach 14 are shown in Fig. 5. Data with the 15-deg ramp configuration are shown for two locations of the hinge line. The measurements are compared with the reference temperature predictions of Eq. (4). The flat-plate data, which remain laminar over the entire measurement domain, compare well with the predicted laminar distribution. On the forward 15-deg ramp, the measurements initially compare well with the laminar reference temperature predictions, but at approximately 120 mm from the leading edge laminar-turbulent transition is occurring, and the heat transfer distribution rises from the laminar predictions to the turbulent predictions. The importance of accounting for the thinning of the reattaching boundary layer, caused by the interaction process, by shifting its virtual origin to the vicinity of reattachment is again stressed.

In the rear ramp experiments, laminar-turbulent transition has been detected in the close vicinity of reattachment[11]; hence, the measured data on the ramp compare well with the respective turbulent reference temperature predictions. It is noted that the solid line reference temperature ramp predictions assume the inviscid pressure level on the ramp. However, a pressure overshoot has been measured just downstream of reattachment (Fig. 4) that, in the case of the 25-deg ramp is significant. Evidently, accounting for the actual pressure distribution in the 25-deg ramp prediction of Fig. 5 yields an improvement in the comparison to the measured heat transfer data.

With reference to Fig. 5, it is also noted that the predictions of Eq. (6) for L_{pk} are in good agreement with the measured distance of the location of peak heating from the reattachment point. The latter has been found, from the comparison of the reference temperature predictions to the ramp heat transfer data, to closely represent the location of the virtual origin of the reattaching boundary layer. In other words, Eq. (6) is seen to provide a good approximation to the effective growth length of the reattaching boundary layer to the location of peak heating.

Furthermore, high-resolution spanwise measurements on the rear 15-deg ramp are shown in Fig. 5 to illustrate that significant spanwise heat transfer variations may occur in reattaching flow regions and downstream. These variations have been attributed to the Görtler instability and the associated formation of contrarotating vortices.[36] However, an extensive parametric study of the resulting heat transfer variations performed in the present investigation[11,12] has shown that, even in the presence of important steady spanwise heat transfer variations, the local turbulent heating level on the ramp is not significantly exceeded. Moreover, when a fully turbulent boundary layer develops over the entire span of the ramp, spanwise heat transfer variations have been found to reduce effectively to zero. A major conclusion of this work[11,12] has, therefore, been that the local turbulent heating level on the ramp, as given by the reference temperature theory (accounting for the actual conditions at the edge of the ramp boundary layer and for the location of its virtual origin), may provide an adequate estimate for an upper limit of the (time-averaged) heat transfer distribution on the ramp downstream of the region of interaction.

Noting the successful application of the reference temperature method to the prediction of the heat transfer distribution (in attached flow regions) over a wide variety of geometries,[11,12] Eq. (5) has been employed to correlate laminar and turbulent peak heating data measured in regions of two- and three-dimensional shock-wave/boundary-layer interactions. The result is illustrated in Fig. 6, where more than 200 data points from 23 references have been assembled.[22] The data cover a Mach number range of 5–20 and five orders of magnitude variation in Reynolds number, which implies a range of shock-wave/boundary-layer interactions from fully laminar cases in the strong viscous interaction regime to transitional and, eventually, fully turbulent cases. The geometries considered include two- and three-dimensional flat-plate/ramp configurations, flat plates with swept or unswept impinging shocks, regions of glancing shock interaction (flat plates with vertical fins), and a double ellipsoid configuration. A laminar boundary layer developing over a flat plate at freestream conditions has been chosen as the reference case in this correlation.

B. Experiments vs Computations

1. Mach 6, 7.5-Deg Ramp Laminar Test Case

The computed pressure distributions for the first test case (Sec. II) are compared with the measured data in Fig. 7. The Dornier computations demonstrate that a grid-independent solution has been attained by the two finest meshes and is in close overall agreement with the measurements. The modest discrepancy (of the order of 10%) observed between the CFD predictions and the measured pressure distribution for a short distance downstream of reattachment lies within the experimental uncertainty. The VKI computations, performed on a similar mesh to the second finest Dornier mesh (noting the different computational domains and grid stretching), also show good agreement with the measured data as well as with the grid-independent Dornier solution (on the two finest meshes).

The corresponding computed skin friction distributions are shown in Fig.8. Clearly, the coarser Dornier mesh performs reasonably well in predicting the skin friction distribution over the attached flow region upstream of the onset of the interac-

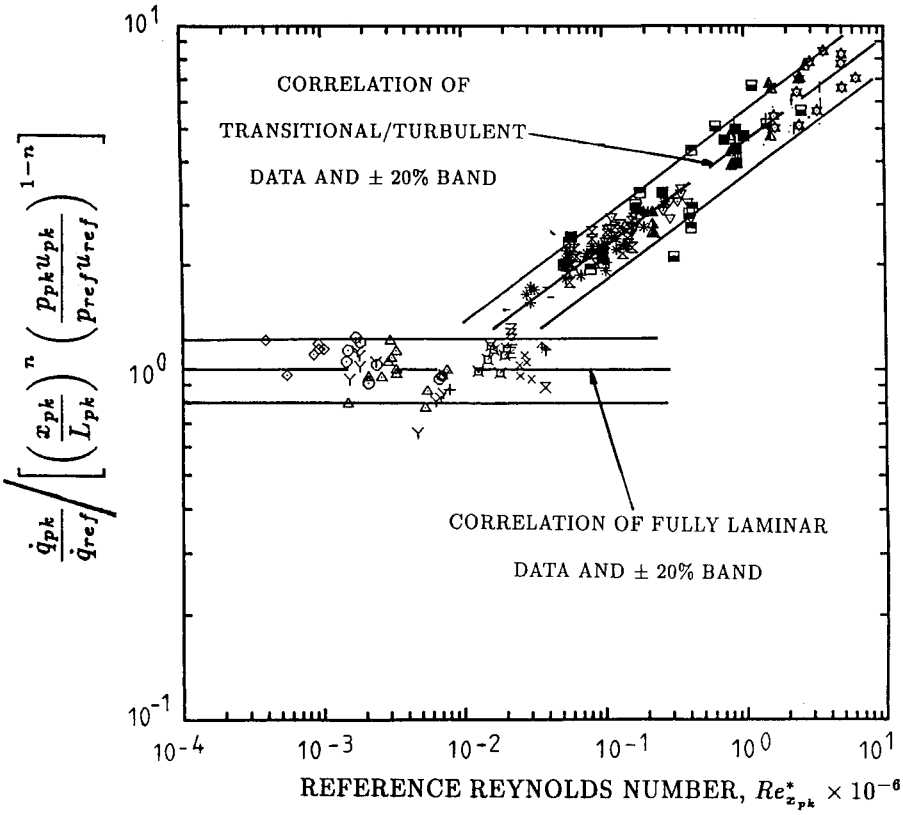

Fig. 6 Correlation of laminar and turbulent peak heating data referenced to laminar flat plate heating level.

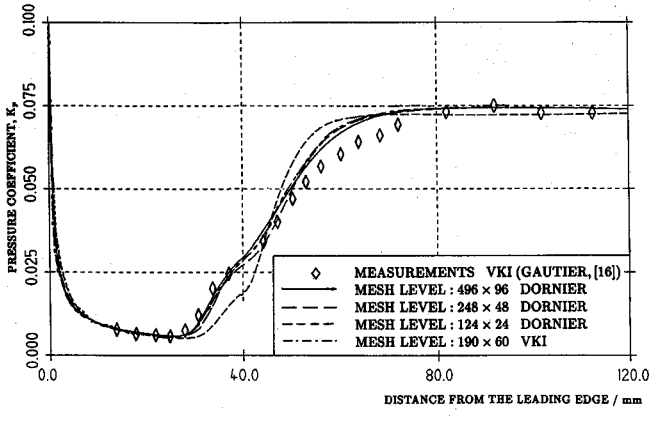

Fig. 7 Comparison of measured and computed pressure distributions over the flat plate/7.5 deg ramp configuration at Mach 6 with $Re_{\text{unit}} = 10 \times 10^6$/m and adiabatic wall temperature.

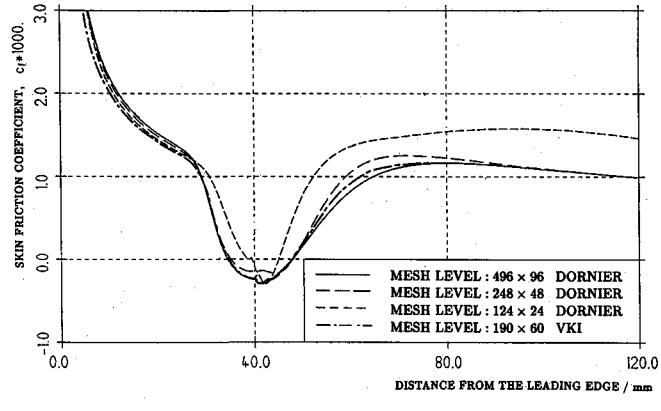

Fig. 8 Computed skin friction distributions over the flat plate/7.5 deg ramp configuration at Mach 6 with $Re_{\text{unit}} = 10 \times 10^6$/m and adiabatic wall temperature.

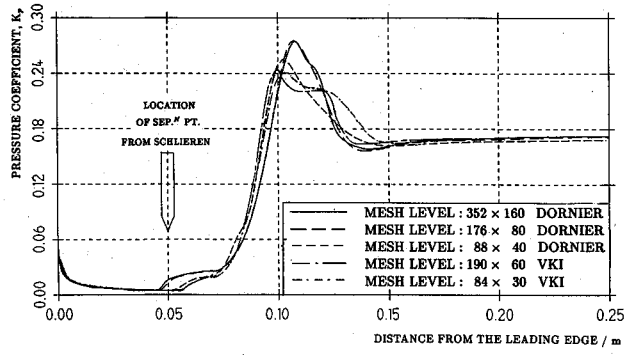

Fig. 9 Computed (laminar) pressure distributions over the flat plate/15-deg ramp configuration at Mach 14 with $Re_{\text{unit}} = 6.5 \times 10^6$/m and $T_w/T_0 = 0.12$.

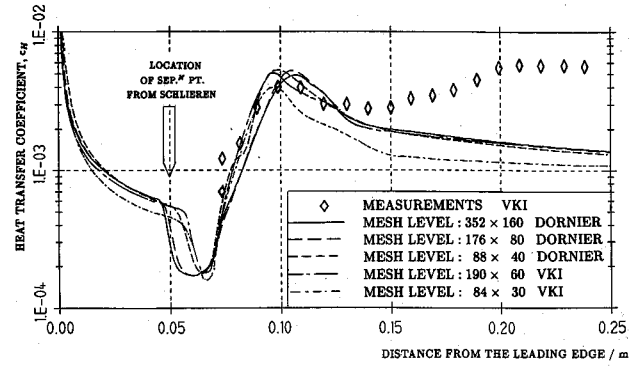

Fig. 10 Comparison of measured and computed (laminar) heat transfer distributions over the flat plate/forward 15 deg ramp configuration at Mach 14 with $Re_{\text{unit}} = 6.5 \times 10^6$/m and $T_w/T_0 = 0.12$.

tion, indicating that the flat-plate boundary layer is adequately resolved and the velocity profile and its gradient at the wall are correctly computed. The correct prediction of the location of the separation point and the extent of the separated region, however, requires the use of highly refined grids.

Concerning time convergence, it is noted that the standard engineering convergence criterion of an L_2 norm reduction in the normalized density residuals by three to four orders of magnitude may be inadequate, and convergence of the location of the separation point may form a more appropriate criterion for separated flow situations. Indicatively, the normalized density residuals in the single mesh VKI computations had to be reduced by six orders of magnitude to achieve the converged (in terms of the location of the separation point) results of Figs. 7 and 8. The multigrid approach employed in the Dornier computations makes use of the coarse grid solutions to accelerate convergence. In this case, the normalized density residuals at the end of the finest grid computation have decreased by three orders of magnitude *relative* to the initial (coarser grid) solution used to start the fine mesh computation.

2. Mach 14, Forward 15-Deg Ramp Laminar Test Case

The computed pressure distributions for the second test case outlined in Sec. II are presented in Fig. 9. The corresponding comparison between the measured and computed heat transfer distributions is shown in Fig. 10. With reference to the Dornier computations, it is noted that a grid-independent solution has again been attained with the two finer meshes, which predicts well the location of the separation point (as determined from the schlieren photograph, Fig. 11) and is in reasonable agreement with the heat transfer measurements on the ramp up to approximately 0.12 m downstream of the leading edge. It is noted that the separation point in the schlieren photograph is allocated at the midpoint between the intersection of the separation shock with the flat plate and the intersection of the separation shock with the bright line representing a line toward the edge of the oncoming boundary layer.

The subsequent discrepancy in Fig. 10 is due to the occurrence of laminar-turbulent transition detected in the experiment,[11] whereas laminar flow has been assumed throughout the computational domain (see also the comparison of the measured heat transfer data to the reference temperature theory, Fig. 5). Transition in this case is occurring a substantial distance downstream of reattachment, and hence it is insignificant to the characteristics of the interaction. In addition, the process is taking place in an almost zero pressure gradient region where, at high Mach numbers, it requires a substantial length to be completed.

The VKI fine grid computation (190×60 mesh points) is seen to underpredict the extent of the interaction and to be in close agreement with the Dornier solution on the 88×40 mesh. As with the Mach 6 test case discussed in Sec. V.B.1, it is recalled that the normal mesh resolution of the VKI fine mesh is very similar to the 40-point resolution of the 88×40 Dornier mesh, due to the different normal extents of the computational domain and the different stretching employed in the two cases. Consequently, there are strong indications that normal mesh resolution is significantly more important than streamwise mesh resolution. To be sure, for a computational domain characterized by a length-to-height ratio of about 4, the VKI meshes involved a ratio of the number of points in the streamwise direction to the number of points in the wall normal direction of the order of 3, whereas the Dornier meshes involved a ratio of only 2. It follows from Figs. 9 and 10 that a mesh point ratio of the order of one-half

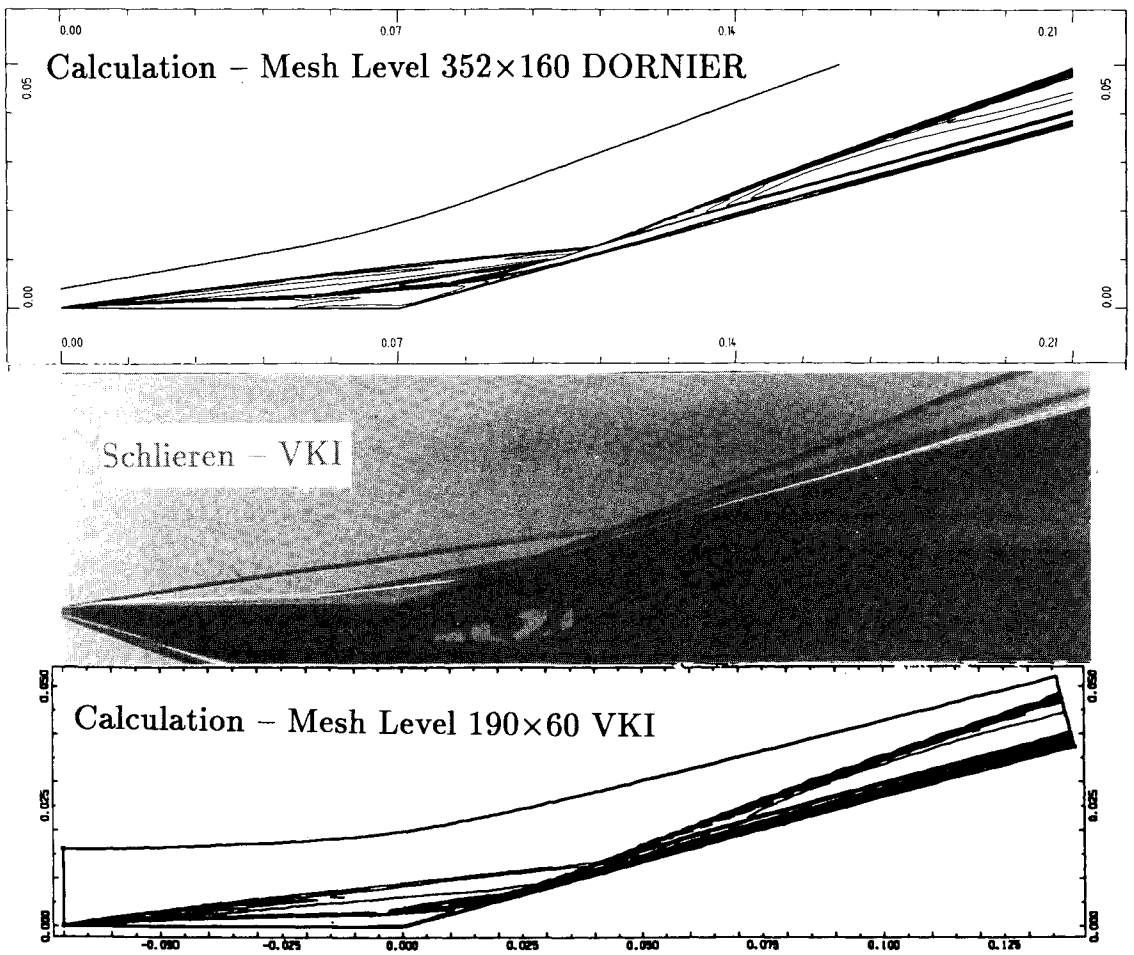

Fig. 11 Comparison of computed (laminar) density contours with the schlieren photograph for the Mach 14 forward 15 deg ramp test case.

(or less) of the length-to-height ratio of the computational domain may be more appropriate for this type of computations. It may also be postulated that the quality of the VKI computations (in terms of the prediction of the extent of the interaction) may be justifiably enhanced if the number of mesh points in the wall normal direction is increased to the detriment of resolution in the streamwise direction.

The importance of grid resolution in the wall normal direction is further manifested by the coarse grid VKI results. Although the pressure distribution in the attached low-pressure gradient regions is well predicted by both codes on all meshes, including the 84 × 30 VKI mesh (Fig. 9), clearly the heat transfer distribution in the latter case is underpredicted relative to the finer VKI mesh computation and the Dornier computations (Fig. 10). It is also noted that all results but the one on the VKI coarse mesh are in good agreement with the reference temperature predictions shown in Fig. 5. This phenomenon has been encountered in many similar high Mach number computations[7,8] and is attributed to an insufficient resolution of the very strong normal temperature gradients in the near wall part of the attached boundary layer.

Finally, a surprising aspect (at first glance) of the comparison between the coarse and fine grid computations of VKI may be that the predicted extent of the interaction is not significantly altered with mesh refinement. This, however, should *not* be viewed as a grid-independent prediction of the location of the separation point, and the poor performance of the coarse grid computation in the attached flow regions (the flow over which is due to strongly influence the interaction/separation characteristics) should be kept in mind.

3. Mach 14, Rear 15-Deg Ramp Transitional Test Case

The measured and computed laminar pressure and heat transfer distributions for the third test case of Sec. II are

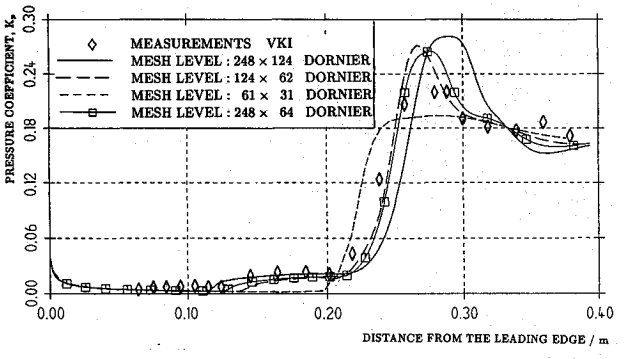

Fig. 12 Comparison of measured and computed (laminar) pressure distributions over the flat plate/rear 15 deg ramp configuration at Mach 14 with $Re_{unit} = 6.5 \times 10^6$/m and $T_w/T_0 = 0.12$.

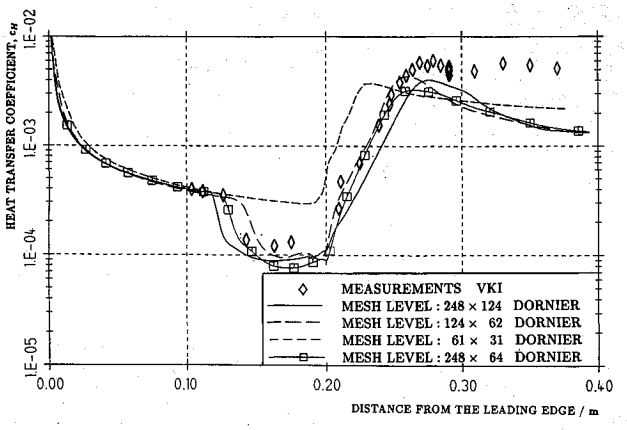

Fig. 13 Comparison of measured and computed (laminar) heat transfer distributions over the flat plate/rear 15 deg ramp configuration at Mach 14 with $Re_{unit} = 6.5 \times 10^6$/m and $T_w/T_0 = 0.12$.

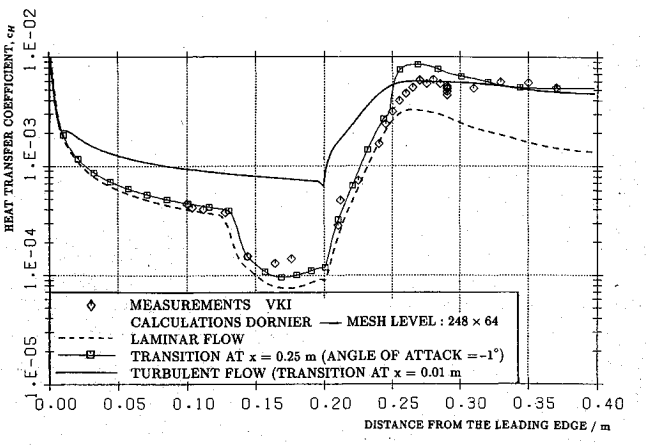

Fig. 14 Comparison of measured and computed heat transfer distributions over the flat plate/forward 15 deg ramp configuration at Mach 14 with $Re_{unit} = 6.5 \times 10^6$/m and $T_w/T_0 = 0.12$, with turbulence model "switched-on" at reattachment.

shown in Figs. 12 and 13. In this case, a grid-independent solution has not been demonstrated, although, on the basis of the Dornier grid-dependence study described in Sec. V.B.2, the finer grid solution (on the 248 × 124 mesh) is believed to closely represent the grid-independent solution. The discrepancies found in the vicinity of peak pressure between the pressure coefficient distributions predicted at different mesh levels is due to the grid dependence of the extent of the separated region and the consequent movement (with grid refinement) of the separation and reattachment shocks and the modification of the interaction between the two.

In addition, it is recalled that the shock-wave/boundary-layer interaction in this case is transitional, in the sense that the boundary layer is laminar at separation but transition has been detected to occur in the close vicinity of reattachment.[11,13] Consequently, the finer grid laminar computation is seen to overpredict the measured extent of the separated region.

Still, the most significant discrepancy between the laminar computations and the transitional experimental data is that the former computations strongly underpredict the measured turbulent heat transfer distribution on the ramp. However, with reference to Fig. 14, good agreement between experiment and computation on the 248 × 64 mesh (as well as with the turbulent reference temperature theory, Fig. 5) is found when "switching on" the turbulence model in the computation just downstream of the predicted laminar reattachment point.

In fact, it follows from Figs. 12–14 that, for cases with laminar oncoming boundary layers, where the interaction process is expected to promote laminar-turbulent transition (most likely in the highly destabilizing reattachment region), the approach adopted herein, of a laminar computation to the reattachment point and switching to a turbulent computation thereafter, may provide an estimate of the most adverse effects of the interaction. Specifically, a grid-independent, fully converged laminar computation is bound to yield the largest possible extent of the interaction and the associated most adverse effect on control effectiveness. Such a laminar computation will also yield the minimum boundary-layer thickness in the "neck" (peak heating) region just downstream of the reattachment compression. This minimum boundary-layer thickness combined with a turbulent computation (starting from the laminar solution at reattachment) will, in turn, yield an upper limit in heat transfer that, on the basis of experimental evidence,[11,12] may not be significantly exceeded even in the presence of significant striation (spanwise) heating variations.

Finally, it is noted that the 1-deg nose-down angle of attack of the configuration has been employed in the "transitional" computation of Fig. 14 (with the turbulence model "switched on" at 0.25 m downstream of the leading edge) only as a crude modeling of the modest (35 μm/55 μm) bluntness of the model

leading edge in the experiment. This angle of attack has been chosen because it yields a pressure rise on the flat plate upstream of the interaction similar to the one induced by the leading-edge bluntness.

VI. Conclusions

A compression ramp database has been assembled from an extensive series of experiments with laminar boundary layers approaching the deflected ramps in the VKI Mach 6 and 14 hypersonic wind tunnels. Among these experiments, only the Mach 6, 7.5-deg ramp experiments[16] and one Mach 14, 15-deg ramp case[11] have exhibited fully laminar interactions and are, therefore, particularly suitable for code validation purposes. The remaining cases have also demonstrated that the laminar oncoming boundary layers are especially prone to separation and that laminar-turbulent transition is promoted by the interaction process, notably by the strong destabilizing effects of adverse pressure gradient and concave flow curvature that characterize the reattachment compression. Furthermore, these experiments have provided a profound insight on the phenomenon of striation heating and have demonstrated[11,12] that the time-averaged local turbulent heating level is not significantly exceeded by peaks in the resulting steady spanwise heat transfer variations, even when these are of the order of $\pm 50\%$.

Analytically, viscous pressure interaction combined with blast wave theory has been found to adequately predict the pressure distribution along flat plates (upstream of the onset of the interaction) induced by the growth of the boundary layer and the finite leading-edge bluntness. Free interaction theory performs well in predicting the plateau pressure level within the separated flow region, and inviscid oblique shock theory gives satisfactory predictions for the downstream ramp pressure level, as well as for the peak pressure attained at the end of the reattachment compression, provided that the type of flow compression is qualitatively known (isentropic, two-shock or single inviscid shock compression).

The reference temperature method has been shown to be very successful in predicting the heat transfer distribution over attached flow regions, both upstream and downstream of the interaction, on the condition that the effective boundary-layer growth length from its virtual origin and the correct flow conditions at the edge of the boundary layer are employed. As a result, a universal correlation law has been developed where, on the basis of the reference temperature theory, more than 200 laminar and turbulent peak heating data have been successfully correlated. Data included in the correlation have been taken over two-dimensional and swept compression ramp and impinging shock configurations, glancing shock interactions, and even a double ellipsoid configuration at Mach numbers between 5 and 20 and over a wide range of Reynolds numbers.

What is currently not possible by analytical or semi-empirical means is the prediction of the location of the separation point and/or the extent of the separated region. This is largely due to the promotion of laminar-turbulent transition by the interaction process, which implies that the development of a correlation law should account for the parameters relevant to the transition process that are currently not well understood.

Finally, on the computational side it has been demonstrated that, in fully laminar interaction cases, full Navier-Stokes solvers are performing very well and may be safely incorporated in the design process, provided that grid-independent solutions are obtained and attention is given to convergence criteria. It has been shown that monitoring of the evolution of the location of the separation point with computational cycles forms a more appropriate (and strict) convergence criterion than the standard monitoring of normalized density residuals. Although turbulence modeling within separated flow regions is not yet sufficiently mature, CFD methods may be employed to provide extreme limits for realistic cases where laminar-turbulent transition is promoted by the reattachment process.

Specifically, a fully laminar computation may provide a maximum extent of the interaction and yield the most detrimental effects on control effectiveness. Thereafter, "switching on" a standard, proven turbulence model in the attached flow region just downstream of reattachment will give an upper limit for the heat transfer distribution on the ramp. It is noted that the (computed) boundary-layer thickness in the "neck" region, which occurs at the end of the reattachment compression, will be smaller in the case of a laminar development of the boundary/shear layer to the reattachment point than it would be if the flow was already turbulent upstream of the interaction. Consequently, the resulting turbulent peak heating level will again represent an upper limit, as it will correspond to the minimum possible thickness of the reattaching boundary layer in the "neck" region.

Acknowledgments

The Mach 14 ramp experiments and the computations were partially supported by Dassault Aviation under the auspices of the Hermes R&D program monitored by P. Perrier. The contribution of J. P. Vermeulen of the VKI toward the development of the peak heating correlation and the striation heating studies is gratefully acknowledged.

References

[1]Perrier, P., and Caupenne, P., "Concepts Generaux Aérodynamiques-aérothermique d' Hermes," *Proceedings of the AGARD-FDP Symposium on Aerodynamics of Hypersonic Lifting Vehicles,* AGARD CP 428, Nov. 1987, Paper 33.

[2]Neumann, R. D., "Missions and Requirements," *Proceedings of the AGARD-FDP-VKI Special Course on Aerothermodynamics of Hypersonic Vehicles,* AGARD Rept. 761, June 1989, Paper 1.

[3]Green, J. E., "Interaction Between Shock Waves and Boundary Layers," *Progress in Aerospace Sciences,* edited by D. Küchemann, Vol. 11, Pergamon Press, Oxford, England, UK, 1970, pp. 235–340.

[4]Hankey, W. L., and Holden, M. S., "Two Dimensional Shock Wave Boundary Layer Interactions in High Speed Flows," AGARDograph 203, June 1975.

[5]Delery, J., and Marvin, J. G., "Shock Wave Boundary Layer Interactions," AGARDograph 280, Feb. 1986.

[6]Bogdonoff, S. M., *Technical Evaluation Report on the Fluid Dynamics Panel Symposium on Aerodynamics of Hypersonic Lifting Vehicles,* AGARD AR 246, April 1988.

[7]Desideri, J. A., Glowinski, R., and Periaux, J. (eds.), *Proceedings of the Workshop on Hypersonic Flows for Reentry Problems,* Pt. I, Antibes, France, Jan. 1990; also *Hypersonic Flows for Reentry Problems,* Vols. I and II, Springer-Verlag, Heidelberg, Germany, 1991.

[8]Desideri, J. A., Glowinski, R., and Periaux, J. (eds.), *Proceedings of the Workshop on Hypersonic Flows for Reentry Problems,* Pt. II, Vol. 3, Antibes, France, April 1991, also *Hypersonic Flows for Reentry Problems,* Vol. III, Springer-Verlag, Heidelberg, Germany, 1992.

[9]Marvin, J. G., "Progress and Challenges in Modeling Turbulent Aerodynamic Flows," *Engineering Turbulence Modelling and Experiments,* edited by W. Rodi and E. N. Ganić, Elsevier, Amsterdam, The Netherlands, 1990, pp. 3–12.

[10]Simeonides, G., "The VKI Hypersonic Wind Tunnels and Associated Measurement Techniques," von Kármán Inst., TM 46, Rhode St-Genèse, Belgium, Nov. 1990.

[11]Simeonides, G., "Hypersonic Shock Wave Boundary Layer Interactions over Compression Corners," Ph.D. Thesis, von Kármán Inst./Univ. of Bristol, Dept. of Aerospace Engineering, Bristol, England, UK, April 1992.

[12]Vermeulen, J. P., and Simeonides, G., "Parametric Studies of Shock Wave Boundary Layer Interactions in Two-Dimensional Compression Corners at Mach 6," von Kármán Inst., TN 181, Rhode, St. Genèse, Belgium, Sept. 1992.

[13]Simeonides, G., and Wendt, J. F., "An Experimental Contribution to the Flat Plate 2D Compression Ramp Shock Wave Boundary Layer Interaction Problem at Mach 14: Test Case 3.7," *Proceedings of the Workshop on Hypersonic Flows for Reentry Problems,* Pt. I, Antibes, France, Jan. 1990; see also *Hypersonic Flows for Reentry Problems,* edited by J. A. Desideri, R. Glowinski, and J. Periaux, Vols. I and II, Springer-Verlag, Heidelberg, Germany, 1991, pp. 129–151; also von Kármán Inst., Preprint 1990-12/AR, Feb. 1990.

[14]Simeonides, G., and Wendt, J. F., "Compression Corner Shock Wave Boundary Layer Interactions at Mach 14, *Proceedings of the*

17th Congress of the International Council of the Aeronautical Sciences, ICAS '90, Stockholm, Sweden, Sept. 1990, pp. 1914–1926; see also von Kármán Inst., Preprint 1990-25/AR, April 1990.

[15]Simeonides, G., and Wendt, J. F., "Fundamental Experimental Studies of Control Effectiveness and Heating at Hypersonic Mach Numbers," *Proceedings of the Ist European Symposium on Aerothermodynamics for Space Vehicles,* European Space Agency, ESA SP 318, May 1991, pp. 143–148; also von Kármán Inst., Preprint 1991-22/AR, June 1991.

[16]Gautier, B., and Ginoux, J. J., "Improved Computer Program for Calculation of Viscous-Inviscid Interactions," von Kármán Inst., TN 82, Rhode St-Genèse, Belgium, March 1973.

[17]Ginoux, J. J., "Supersonic Separated Flows over Wedges and Flares with Emphasis on a Method of Detecting Transition von Kármán Inst., TN 47, Rhode St-Genèse, Belgium, Aug. 1968.

[18]Hayes, W. D., and Probstein, R. F., *Hypersonic Flow Theory,* Academic Press, New York, 1959, Chap. 9.

[19]Lukaciewicz, J., "Hypersonic Flow—Blast Wave Analogy," Arnold Engineering Development Center, TR-61-4, Arnold AFB, TN, 1961.

[20]Eckert, E. R. G., "Engineering Relations of Friction and Heat Transfer to Surfaces in High Velocity Flow," *Journal of Aerospace Sciences,* Vol. 22, No. 8, 1955, pp. 585–587.

[21]Neumann, R. D., and Hayes, J. R., "Introduction to Aerodynamic Heating Analysis of Supersonic Missiles," *Tactical Missile Aerodynamics,* edited by M. J. Hemsch and J. N. Nielsen, Vol. 104, Progress in Astronautics and Aeronautics, AIAA, New York, 1986, pp. 421–481.

[22]Simeonides, G., and Vermeulen, J. P., "Identification of Relevant Parameters and Revision of Peak Heating Correlations for Hypersonic Two- and Three-Dimensional Shock Wave Boundary Layer Interactions, *Proceedings of Meeting on Hypersonic Aerodynamics*, EuroMech 289, Aachen, Germany, April 1992; also von Kármán Inst., Preprint 1992-16/AR, May 1992.

[23]Bushnell, D. M., and Weinstein, L. M., "Correlation of Peak Heating for Reattachment of Separated Flows," *Journal of Spacecraft and Rockets,* Vol. 5, No. 9, 1968, pp. 1111, 1112.

[24]Hung, F. T., "Interference Heating due to Shock Wave Impingement on Laminar Boundary Layers," AIAA Paper 73-678, July 1973.

[25]Hung, F. T., and Barnett, D. O., "Shock Wave Boundary Layer Interference Heating Analysis," AIAA Paper 73-237, Jan. 1973.

[26]Haase, W., Wagner, B., and Jameson, A., "Development of a Navier-Stokes Method Based on a Finite Volume Technique for the Unsteady Euler Equations," *Proceedings of the 5th GAMM Conference on Numerical Methods in Fluid Mechanics,* edited by M. Pandolfi and R. Piva, Vol. 7, Notes on Numerical Fluid Mechanics, Vieweg, Braunschweig, Germany, 1983, pp. 99–107.

[27]Haase, W., "Solution of the Navier-Stokes Equations for Subsonic and Supersonic Flows in Rarefied Gases," *Proceedings of Numerical Simulation of Compressible Navier-Stokes Flows,* edited by M. O. Bristeau, R. Glowinski, J. Periaux, and H. Viviand, Vol. 18, Notes on Numerical Fluid Mechanics, Vieweg, Braunschweig, Germany, 1987, pp. 139–157.

[28]Haase, W., and Echtle, H., "Computational Results for Viscous Transonic Flow Around Airfoils," AIAA Paper 87-422, Jan. 1987.

[29]Haase, W., "Viscous Hypersonic Flows over Compression Ramps," *Proceedings of the 8th GAMM Conference on Numerical Methods in Fluid Mechanics,* edited by P. Wesseling, Vol. 29, Notes on Numerical Fluid Mechanics, Vieweg, Braunschweig, Germany, 1990, pp. 189–200.

[30]Haase, W., "2D Hypersonic Ramp Flow," *Proceedings of the Workshop on Hypersonic Flows for Reentry Problems,* Pt. II, edited by J. A. Desideri, R. Glowinski, and J. Periaux, Vol. 3, Antibes, France, April 1991; also *Hypersonic Flows for Reentry Problems,* Vol. III, Springer-Verlag, Heidelberg, Germany, 1992, pp. 368–379.

[31]Manna, M., "A 3-D High Resolution Upwind Finite Volume Euler Solver," von Kármán Inst., TN 180, Rhode St-Genèse, Belgium, April 1992.

[32]Manna, M., "Validation of Central and Upwind 3D Compressible Flow Solvers," *Computational Fluid Dynamics,* von Kármán Inst., LS 1992-04, Rhode St-Gènese, Belgium, March 1992.

[33]Manna, M., Deconinck, H., Ma, E., and Li, C. P., "A Comparison of High Resolution Upwind Solvers on 3D Inviscid Hypersonic Flow," *Proceedings of the AGARD-FDP Symposium on Theoretical and Experimental Methods in Hypersonic Flows,* AGARD CP 514, May 1992, Paper 41.

[34]Cebeci, T., and Smith, A. M. O., *Analysis of Turbulent Boundary Layers,* Academic Press, New York, 1974.

[35]Stock, H. W., and Haase, W., "Determination of Length Scales in Algebraic Turbulence Models for Navier-Stokes Methods," *AIAA Journal,* Vol. 27, No. 1, 1989, pp. 5–14.

[36]Ginoux, J. J., "On Some Properties of Reattaching Laminar and Transitional High Speed Flows," von Kármán Inst., TN 53, Rhode St-Genèse, Belgium, Sept. 1969.